Bull Eng Geol Environ (2016) 75:1377–1397
DOI 10.1007/s10064-015-0798-6

ORIGINAL PAPER

Quantitative rockfall risk assessment for an important road by means of the rockfall risk management (RO.MA.) method

P. Budetta[1] · C. De Luca[1] · M. Nappi[1]

Received: 7 April 2015 / Accepted: 18 September 2015 / Published online: 6 October 2015

Abstract This paper deals with a quantitative risk analysis, performed using the rockfall risk management (RO.MA.) method, for a road affected by rockfalls. This approach allows evaluating the rockfall risk, also considering existing protection devices. Rockfall hazard and risk were assessed for an important and very busy road stretch linking Positano to Amalfi in the Campania region of southern Italy. An estimate of the rockfall return periods for assigned volume classes was obtained using the magnitude–frequency curves (MFCs) computed through the analysis of a rockfall inventory covering a time span from 1996 to 2008. For rockfall volumes of 0.1, 1.0, and 10 m^3, using a 2D trajectory simulating code, the involved kinetic energies and run-out distances of boulders that may hit the road were calculated. The risk, expressed as the annual probability of a fatal accident for the three rockfall hazard scenarios has been evaluated both without and with protection devices, respectively. The total final risk is given by the sum of partial risks related to the three scenarios. The analysis showed that regardless of whether there are any rockfall protection devices, the total risk remains almost constant. This is due to the wide spread of slopes protected with inadequate restraining metallic nets characterized by decreasing catching capacities, as possible rockfall magnitude increases. The individual risk is not acceptable, and some actions are requested in order to lower it.

✉ P. Budetta
paolo.budetta@unina.it

[1] Department of Civil, Architectural and Environmental Engineering, University of Naples ''Federico II'', Piazzale Tecchio, 80, 80125 Naples, Italy

Keywords Rockfall hazard · Quantitative risk analysis · Event tree analysis · Roads · Southern Italy

Introduction

With reference to landslides, the quantitative risk analysis (QRA) affecting roads includes the evaluation of several interconnected factors, such as hazard causes and their assessment, elements at risk, road and vehicle vulnerability, risk estimation, and evaluation of the acceptable risk (Corominas et al. 2014). Furthermore, considering the possible presence of protective measures that are able to reduce the risk level, their efficiency also must be evaluated. Because of the amount of qualitative and quantitative data required, QRA is very hard to perform and, in consequence, simplifying assumptions must be considered.

For rockfalls affecting roads, average frequencies of blocks of various size landing, and then either staying in the roadway or passing through, can be used to determine the probability of each event occurring during an assigned time period (Roberds 2005). These average frequencies are hard to calculate, because they depend on several variables, such as probable block volume detached per year along the slope impending over the road, fragmentation phenomena, run-out distances, topographical characteristics of slopes, as well installed protection devices. Databases reporting reliable information that concern previous rockfalls (number, magnitude, and related damages), during a prefixed time interval, must be available (Hungr et al. 1999; Dai et al. 2002; Malamud et al. 2004). Unfortunately, detailed inventories are missing because road administrations only record the most serious events or life threatening ones. Otherwise, by means of 2D and/or 3D trajectory simulations, it is possible to evaluate the percentage of all

trajectories that could intersect the road (Jaboyedoff et al. 2005).

According to Peila and Guardini (2008), the probability that a falling rock hits a moving vehicle on a road $P(R)$ may be calculated as the product of the generic probability for one vehicle to be hit by a rock $P(A)_v$ and the number of vehicles travelling on the road per year $Nv_{/a}$. $P(A)_v$ is given by:

$$P(A)_v = P(S) \cdot P(T|S) \quad (1)$$

where $P(S)$ is the probability of spatial correspondence between the rock and the vehicle and $P(T|S)$ is the conditional probability of temporal correspondence between the rock and the vehicle. Once $P(R)$ has been evaluated, it is necessary to calculate the probability that, as a result of the impact, at least one occupant of the vehicle is killed (fatal accident).

Related consequences (vulnerability) include casualties, property damages, delays for road closures, and costs. Many other factors, such as traffic volume, sight distance, vehicle speed, number of occupants and their position in the vehicle, and type of vehicle, affect this estimation (Bunce et al. 1997; Roberds 2005). The road vulnerability degree also depends on the interaction between travelling vehicles and landslide debris. Bunce et al. (1997) identified three possible interactions between rocks and vehicles: moving vehicle/falling rock, moving vehicle/fallen rock, and stationary vehicle/falling rock. For simplicity, we assume that vehicles are evenly distributed in time and space, and that all vehicles have the same length. Also, certain traffic data, such as annual average, daily or diurnal and evening seasonal traffic, vehicle types, and speeds, should be available. Nevertheless, only for the most important and very busy roads are these data recorded, and for many mountainous roads (where more frequently rockfalls happen) traffic records are missing. At last, also the damage to paving due to rock impacts, which may cause damage to vehicles or accidents due to sudden changes of direction, affects the vulnerability.

The annual probability of loss of life to an individual (e.g., the most exposed one to rockfalls) is generally given by multiplying the annual probability of occurrence of a rockfall event (of a given magnitude) by the probability of a falling rock hitting the vehicle, and by the vulnerability of the person given a block of size m impacting the vehicle (adapted from Fell et al. 2005). The expected number of casualties for year for different hazard scenarios can be also calculated combining the damage functions in order to determine the direct and then indirect consequences for a given time period, in the manner suggested by Roberds (2005). Less frequently the risk is expressed as annual monetary loss per kilometer or the annual probability of road damage (Corominas et al. 2014). Lastly, the individual risk for different rockfall hazard scenarios must be compared with the recommended descriptors for risk zoning (AGS 2007; Ferlisi et al. 2012).

The numerical evaluation of the above-mentioned elements concerning hazard, vulnerability, and risk, frequently implies some simplifications, approximations, and the use of expert judgments (heuristic approaches). Input data are critical factors and the degree of approximation of results to be obtained depends on the quality of many variables, such as the size of the study area, the availability of topographic maps and their scales, the experience of geological surveyors, and the availability of monetary funds (Corominas et al. 2014). In spite of the uncertainty of assessments, in the literature several examples of QRA applications to roads and railroad tracks exposed to fast landslides (mainly rockfalls and debris flows) have been proposed (Bunce et al. 1997; Hungr et al. 1999; Budetta 2002; Archetti and Lamberti 2003; Guzzetti et al. 2004; Peila and Guardini 2008; Ferlisi et al. 2012; Michoud et al. 2012; Mignelli et al. 2012; Jaiswal and van Westen 2013; Mignelli et al. 2014). Some of the above-mentioned studies are based on the analysis of the rockfall recurrences, determined from the landslide magnitude-frequency curves (MFCs), and on the results of physically based, spatially distributed rockfall simulation models (Bunce et al.1997; Hungr et al.1999; Guzzetti et al. 2004). In order to evaluate interconnected probabilities, Budetta (2002) and Peila and Guardini (2008) made use of the event tree analysis that is a logical process able to examine cause–effect interconnections arising from the triggering of fast landslides (debris flows and rockfalls, respectively). Sometimes, rockfall historical data, photogrammetric surveys, and digital elevation models (DEMs) are analyzed and manipulated in workstation platforms (Guzzetti et al. 2004; Mignelli et al. 2014); otherwise, suitable "Slope Angle Distribution" procedures, regarding cliff units at a regional scale with their normalized cumulative distribution functions, are used (Michoud et al. 2012). Jaiswal and van Westen (2013) made a quantitative analysis of landslide hazard and risk, and subsequently inserted in different landslide risk reduction strategies that concern road stretches and railroad tracks in India.

The aim of this paper is to show the results of a QRA application to the road sections belonging to an important road, the main one linking some resorts in the southern slope of the Sorrento Peninsula (southern Italy), namely Positano, Amalfi, and Salerno (Fig. 1). High traffic intensity affects this road, which, due to its complex geological setting, is sometimes affected by rockfalls, causing damage, injuries, and road closures (Budetta and Nappi 2013). Ferlisi et al. (2012) already studied risk conditions affecting this road and analyzed three risk scenarios based on the possible interactions between rocks and vehicles, in the

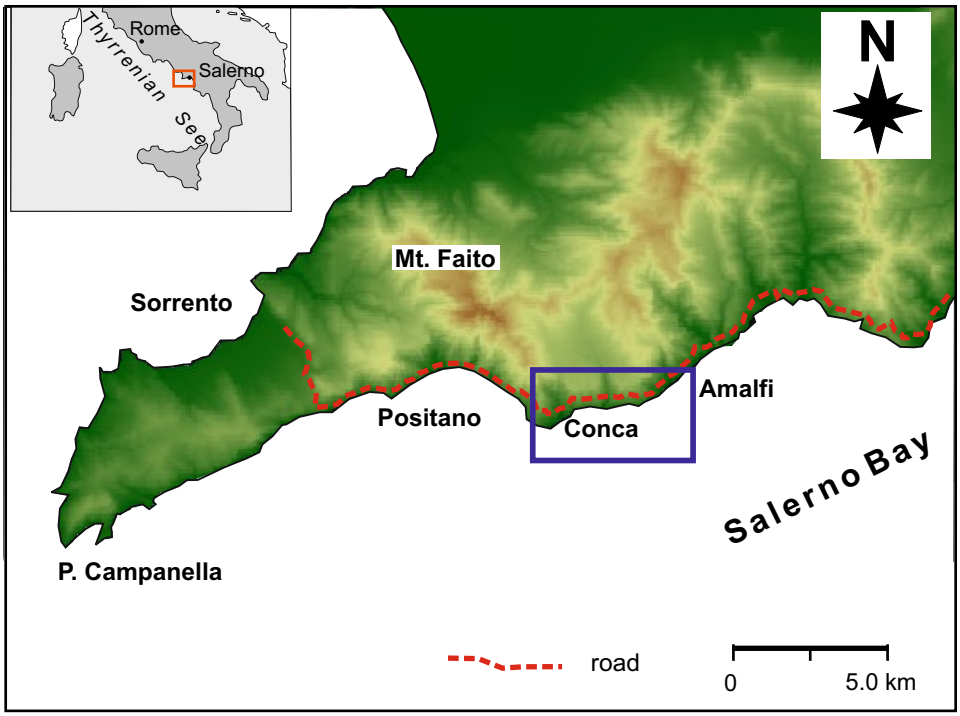

Fig. 1 Location of the studied area

way suggested by Bunce et al. (1997). They concluded that, even though the individual rockfall risk to life is tolerable for the entire road length (about 34 km), there are some road stretches (mainly affected by higher average rockfall frequencies) where the above risk is not acceptable. However, they did not find their analysis on rockfall simulation models and did not took into account the existing protection measures on some road cuts, and the level of risk reduction they may produce. Consequently, on the basis of detailed geo-structural and geo-mechanical data concerning the rock masses impending over the studied road, rockfall inventories, traffic data, and trajectory simulations, risk values affecting ten road sections were estimated in this paper, taking into account three possible hazard scenarios based on the rockfall magnitude, as well the presence of rockfall protection devices and their efficiency.

The adopted method

QRA application was performed using the rockfall risk management (RO.MA.) method by Peila and Guardini (2008). Available data regarding rockfall frequencies, traffic, and existing protection devices have been taken into account, and the risk, expressed as the number of fatalities per year and per kilometer, has been then calculated. The method develops through five steps, including (Fig. 2) identification of unstable areas and the number of rocks per year that may hit the road (*Nr*); road vulnerability assessment; event tree analysis; risk assessment; evaluation of the efficiency of rockfall protective measures; and calculation of the residual risk (Peila and Guardini 2008; Mignelli et al. 2014). The number of boulders that may hit the road (*Nr*) or that may stop upstream (*Ns*), is obtained from field data or, alternatively, through trajectory simulations (Jaboyedoff et al. 2005). By means of the event tree analysis (Fig. 3), the complete sequence of events which may result from a landslide until the killing of a road user (fatal accident) is evaluated from a probabilistic point of view. For the above-mentioned approach, the required input data concern the number of rocks hitting the road per year (*Nr*), the length of the hazardous road stretch (*Lr*), the average (or limit) speed of the vehicles (*Vv*), the average vehicle length (*Lv*), and the number of vehicles travelling on the road per day (*Nv*) (Peila and Guardini 2008). In order to evaluate the probability of a travelling vehicle hitting a previously fallen rock, it is necessary to introduce the decision sight distance (DSD). The conditional probability of temporal correspondence between the rock and the vehicle [$P(T|S)$] can be assumed equal to the part of the year occupied by a single passing of the vehicle through the road section. Successively, it is necessary to consider the probability that the rock damages the road paving and a consequent fatality may derive from this event (probability per year of death due to a damaged road paving). For these probabilities, Peila and Guardini (2008) stated values that were inferred from data of the Italian Institute for Statistics

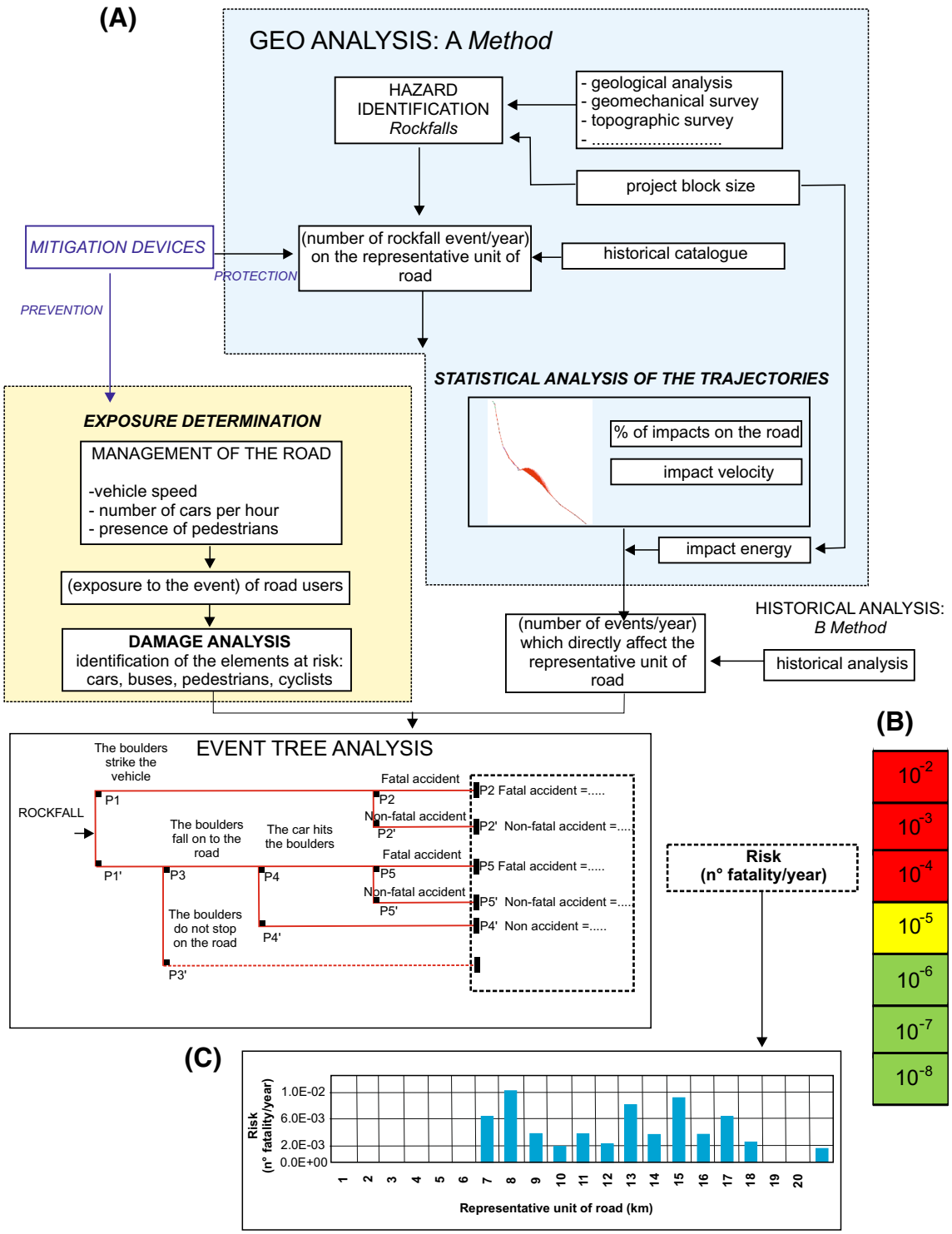

Fig. 2 **a** Procedural flow chart for rockfall risk management assessment. **b** Abacus defining the threshold values of rockfall risk. Acceptable values are in the *green lower* portion of the figure. Unacceptable risk values fall in the *upper red* portion of the figure. **c** Histogram representing risk values for the representative road sections. After Peila and Guardini (2008) and Mignelli et al. (2014) modified

(ISTAT) regarding the causes of road accidents on the entire Italian road network. The event tree analysis develops along 12 different paths (Fig. 3), and the probability of occurrence of each can be calculated from the product of each single event that constitutes the path itself. The final value of each path is given by the sum of probabilities

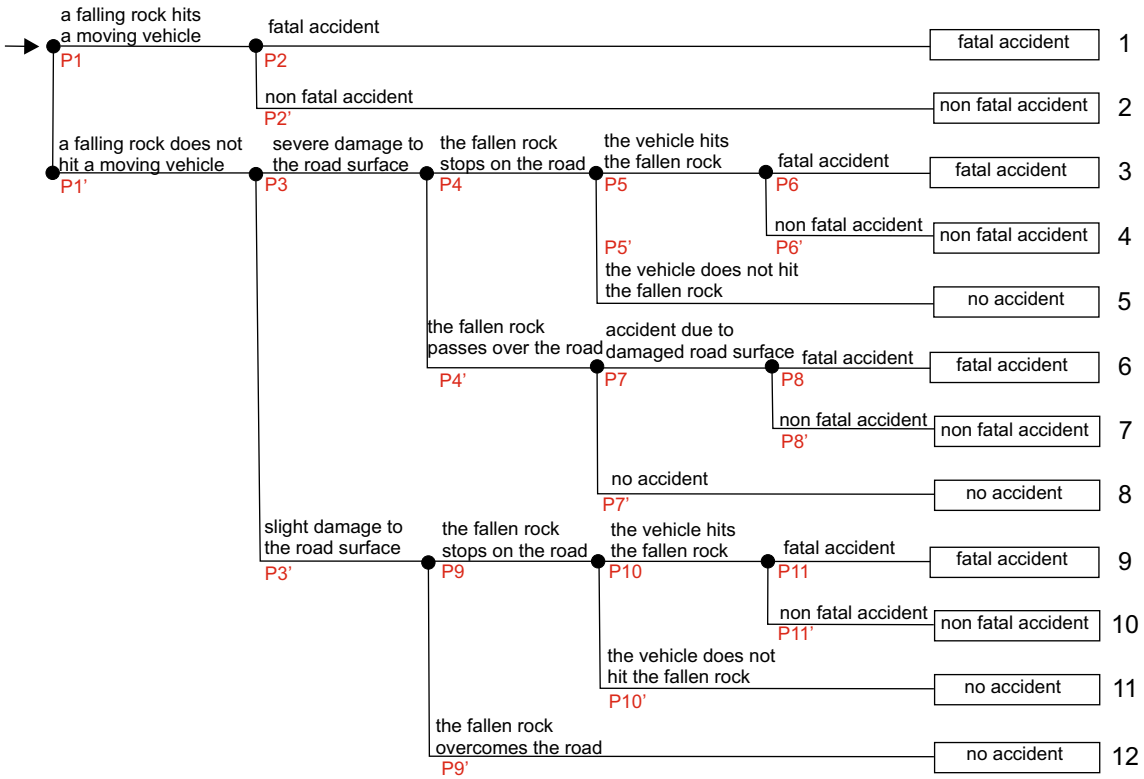

Fig. 3 General scheme of the event tree proposed for the analysis of the probability of a fatal accident due to a rockfall on a road. Modified from Peila and Guardini (2008)

concerning paths with the same final result (i.e., fatal accident, non-fatal accident, and no accident). The next step deals with the ability of protection measures to stop the falling rocks (efficiency), reducing the number of those who may hit the road per year. The number of retained block ($N'r$) can be calculated on the basis of the catching capacities of installed devices (shelters, embankments, rockfall barriers, mesh drapes, etc.). If we implement $N'r$ in the event tree, it is possible to estimate new probability values concerning fatal accidents. Finally, these last risk values can be compared either with the previously calculated average value or with risk criteria defined in the international literature (AGS 2007; Mignelli et al. 2014). In this respect, Mignelli et al. (2012) suggested the use of an abacus defining the threshold values of acceptable and unacceptable rockfall risks (Fig. 2).

The road stretch studied

The studied road portion belongs to a very difficult road path (Fig. 1) going along the coast (the Amalfitana no. 163 state road) that was built in the middle of the nineteenth century. Because of the presence of very steep slopes and limited available space, the road is characterized by only one single lane going in each direction and a high degree of road curvature resulting in a small DSD. The width of the road is 7.0 m, and the imposed speed limit is everywhere 50 km/h.

The studied road stretch, 3.045 km long (from 23+625 to 26+670 km, where kilometers increase progressively towards Salerno) and crossing Conca dei Marini municipal territory, was chosen because, in time, it is the one most affected by rockfall events. The road has been subdivided into 10 sections, with lengths varying between about 225 and 380 m, defined so as to have—as much as possible—overlooking slopes characterized by homogeneous geological characteristics. Protection devices constituted by rockfall barriers, reinforced wire rope nets and mesh drapes, installed by ANAS (the national company administrating the road), are present along some slopes and cuts belonging to the studied road sections (Fig. 4; Table 1). These passive protections, generally installed after every new rockfall, prevent the boulders to gain velocity or keep them from flying outward the slope impending over the road, limiting their run-out distances.

By means of topographic maps and field measurements, the Actual Sight Distance ASD (km) for the 10 sections, in both directions, was calculated by the following (Ministerial Decree 5/11/2001 no. 6972):

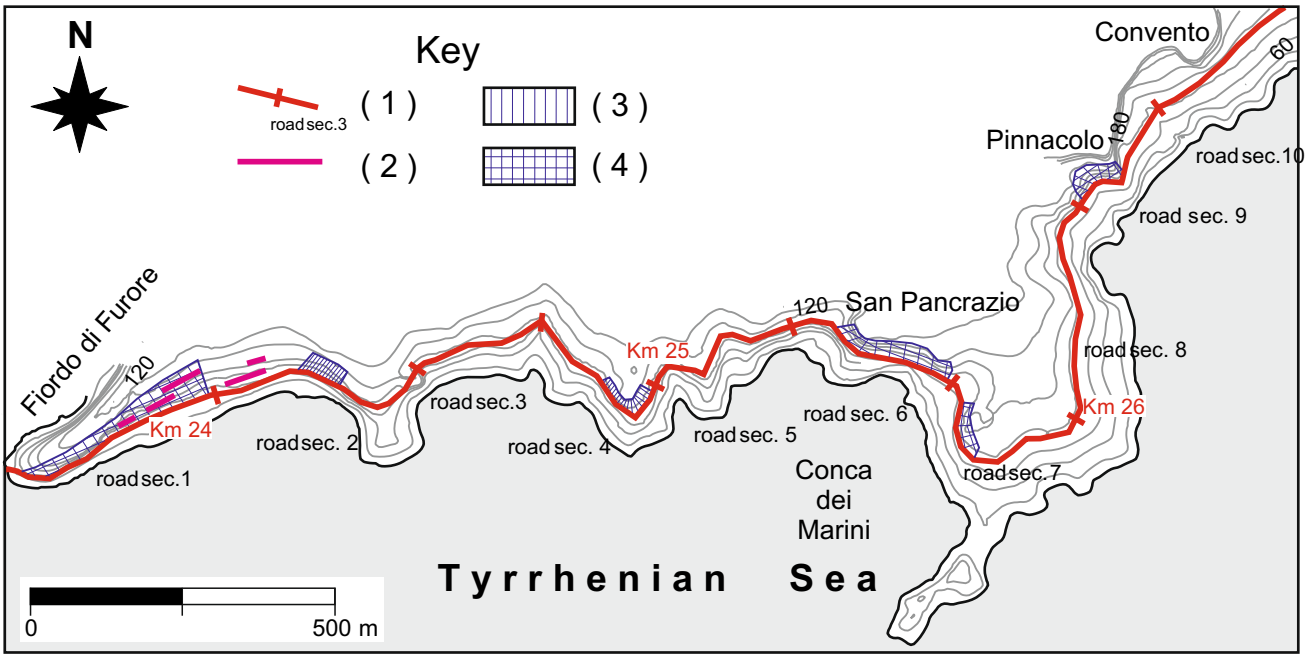

Fig. 4 The studied road stretch. Key *1* Road track and related road sections; *2* rockfall barrier; *3* drapery mesh; *4* reinforced wire rope net

Table 1 Length of the studied road sections, rockfall events recorded during the time span 1996–2008, mean failure frequency, and types of installed protection devices

Road section no.	Road length (km)	Rockfall events No.	Mean failure frequency−λf (events year^{-1} km^{-1})	Protection devices	Length of the protected slopes (km)
1	0.375	1	0.205	Rockfall barriers and reinforced wire rope nets	0.375
2	0.360	1	0.214	Drapery mesh	0.075
3	0.225	1	0.341	–	–
4	0.275	0	0	Drapery mesh	0.150
5	0.280	3	0.824	–	–
6	0.310	2	0.496	Reinforced wire rope nets	0.220
7	0.350	0	0	Reinforced wire rope nets	0.110
8	0.380	0	0	–	–
9	0.230	5	1.672	Reinforced wire rope nets	0.110
10	0.260	2	0.591	–	–

$$\mathrm{ASD} = 2\sqrt[2]{2R(b+c)}, \tag{2}$$

where R is the radius of the curvature of the road (measured by the 1:2000 scale topographical map), b the distance between the driver's eye and the edge of the road curve, and c the distance between a possible boulder placed on the lane and the edge of the road curve.

Only in cases where considerable obstacles or vegetation caused sight distances to become critical, b values were measured using levelling rods. For the sake of simplicity, the supposed boulder position on the road was always assumed at $c = 3.50$ m from the road edge, this distance being half of the road width (the road centerline). The percentage of reduction in the decision sight distance (PDSD) is given by:

$$\mathrm{PDSD} = \frac{\mathrm{ASD}}{\mathrm{DSD}} 100\,\%, \tag{3}$$

where ASD is the actual sight distance and DSD represents the length of road (km) a driver needs in order to make a complex or instantaneous decision.

In Italy, DSD is considered the distance along a roadway within which a 15-cm high stationary object is continuously visible from a height of 1.10 m above the road

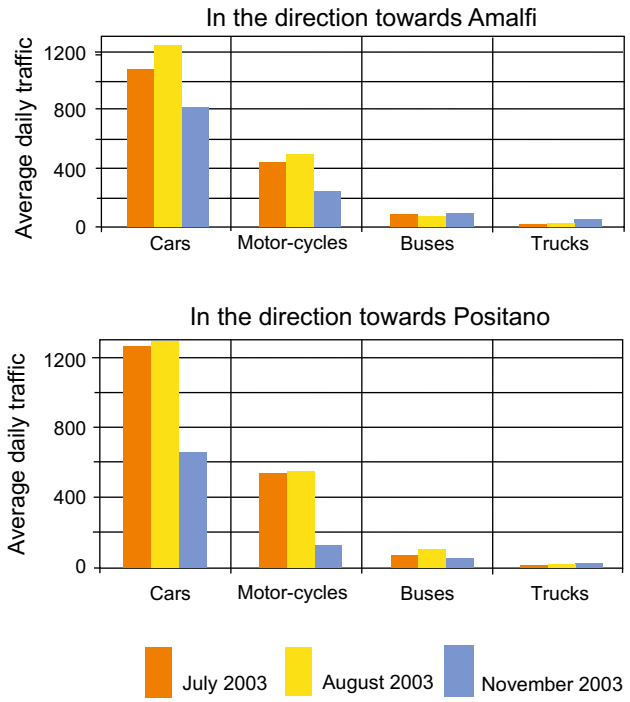

Fig. 5 Average daily traffic (ADT) during the given observation period (2003) (after Cantarella and De Luca 2006 modified)

(Ministerial Decree 5/11/2001 no. 6972). PDSD values obtained using Eq. (3) for all sections, vary between 38 and 30 %, and they are always very limited.

Traffic data (Fig. 5) were recorded in the spring/summer and the autumn/winter periods of 2003, with reference to different sunlight conditions (day and night), by Cantarella and De Luca (2006). About 80 % of the traffic is made up of cars and the remainder of motorcycles and tourist coaches. During the two above-mentioned periods, relevant differences were not recorded and the average daily traffic (ADT) was almost constant because the traffic due to commuting and business, intense in the low season, is substituted by an equally intense tourist one, during the spring/summer period. Since the traffic is mainly made up of cars (Fig. 5), the average number of these vehicles travelling on the road per day (*Nv*), amounting to 1058 in all the road sections and in the two directions (towards Positano and Amalfi), was taken. At last, pedestrian traffic on the road is negligible.

Geological and geo-mechanical setting

The road crosses a coastal area characterized by high reliefs lying on the northern side of the Gulf of Salerno. This area belongs to the Sorrento-Amalfi peninsula, which is a carbonatic horst transversal to the Southern Apennine chain, separating two tectonic depressions—the Campania Plain to the north and the Gulf of Salerno to the south (Bonardi et al. 2009). This horst is bounded by major NE–SW-trending faults, and is also affected by several minor NW–SE transverse faults (partly strike-slip faults) creating secondary horst-graben structures. As a result of the heavy tectonic disturbance, the outcropping rock masses are always very fractured.

Because of the near vertical cliffs and very steep slopes, in a small distance from the coastline, the relief goes from the sea level until to heights greater than 600 m ASL with mean slope angles of about 40° (Fig. 6). The studied road stretch is bounded towards the west by a deep rias, called *Fiordo di Furore*, which extends itself along an important

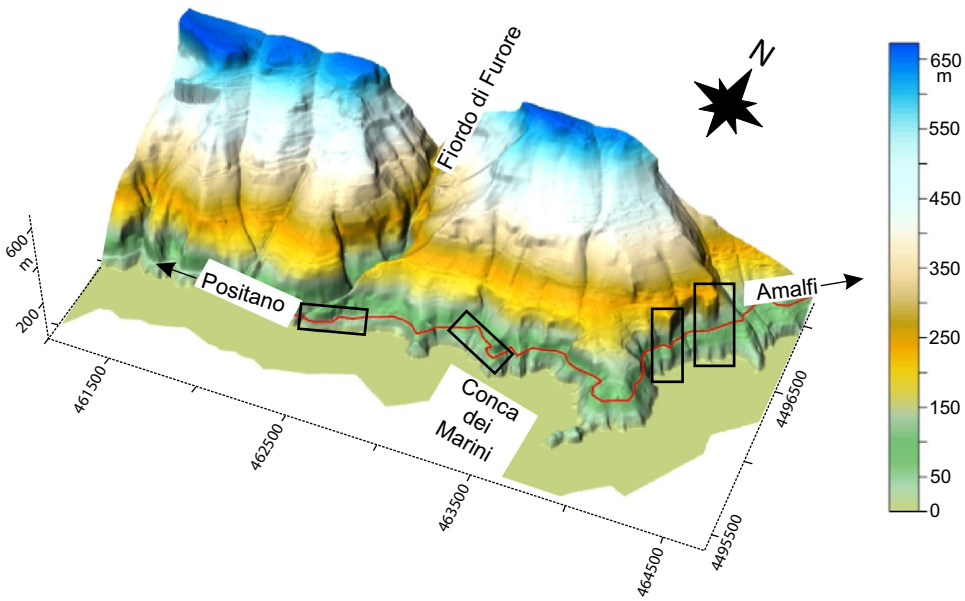

Fig. 6 3D map showing the topography of the studied area with the road path. The areas studied in detail are highlighted with *black rectangles*. The *Fiordo di Furore*, a deep rias that extends itself along an important strike slip fault defines the studied road stretch towards the west

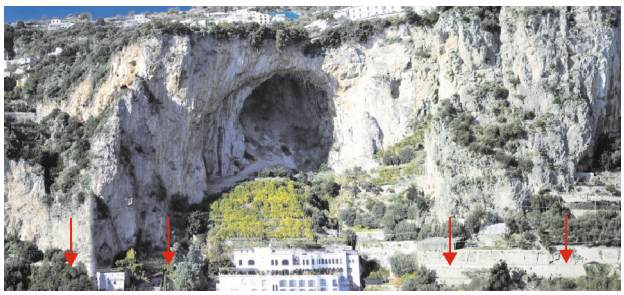

Fig. 7 The wide karst cavity at Conca dei Marini, where the studied road stretch ends. The *red arrows* show the road path

N–S-oriented strike-slip fault (Fig. 6), whereas towards the east, it ends below a wide karstic cavity carved in Pleistocene cemented breccias (Fig. 7). Generally, slopes immediately impending over the road appear to be near vertical, while the more distant slopes have a lower overall steepness (40°–50°), though small isolated cliffs appear, with heights ranging between 10 and 30 m (Di Crescenzo and Santo 2007). Almost vertical slope profiles favour the free fall of boulders on the road, whereas in the remaining cases irregular rock faces, due to the presence of ridges or benches with lower slope angles, cause launching and rebounding phenomena. Several steep slopes have been terraced using traditional dry gravity walls ("*macerine*") to enable the local citrus fruit trees to be cultivated. These terraces have a great influence on the rebound heights and endpoints of falling boulders (see below).

On the slopes flanking the road, cross-bedded Jurassic limestones and dolomitic limestones outcrop, sometimes dipping less than the slope in the directions SW and SE or with horizontal strata (Fig. 8). The tectonic disturbance promotes possible wedge and/or plane failures along the joint set intersections and stratification. Locally, in areas of medium–low steepness, such as terraces and wide level surfaces, silty-sandy volcanic ashes and sandy gravels, mixed with highly weathered pyroclastic sediments can be found, dating back to the Holocene. Pleistocene cemented breccias made of coarse fragments of carbonate rocks and affected by tectonic disturbance are also present (Figs. 7, 8).

With reference to rock masses flanking the entire road stretch, generally three joint sets can be found corresponding to fractures striking parallel to slopes or with mutually intersecting NW–SE and NE–SW trends. The joint spacing ranges between 600 and 2000 mm and tectonic discontinuities are open and very open joints (1–10 cm), almost all filled with pyroclastic materials. In several sites, cavities and very open joints are present, due to the chemical dissolution of limestones. Thus, karst dissolution proves to be an active geomorphological process weakening over time the rock bridges connecting adjacent rock blocks.

The geo-mechanical setting of two unstable slopes has been studied in detail (Figs. 9, 10). These sites were selected because they are representative of different slope geometries and failure conditions affecting boulder detachment areas and their trajectory paths hitting the road. Slope geometries have been carefully characterized using photogrammetric surveys (original scale 1:500) based on photographs collected from an helicopter. Given the difficult accessibility to slopes, the quantitative and qualitative description of discontinuities (orientation, spacing, persistence, aperture, infilling materials, and roughness of joint surfaces) has been carefully performed by rock-climber geologists. Geo-structural and geo-mechanical surveys were performed according to the suggested methods by ISRM (2007) and Palmstörm (1996). The collected data in

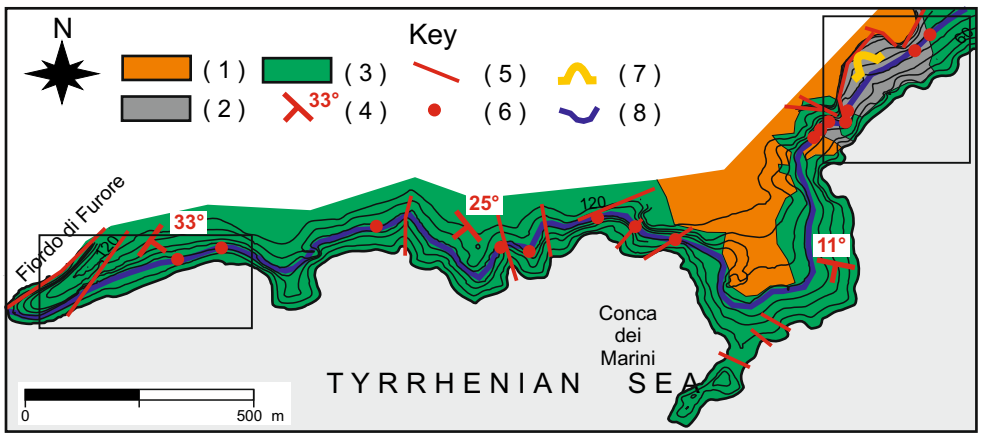

Fig. 8 Geological map of the studied area. (*1*) Silty-sandy volcanic ashes and sandy gravels, locally mixed with highly weathered pyroclastic sediments—Holocene (*2*) Cemented breccias made of coarse fragments of carbonate rocks—Pleistocene (*3*) Well-stratified or massive limestones and dolomitic limestones—Mesozoic (*4*) Attitude of bedding planes and related dip angles (*5*) Fault (*6*) Rockfall event (*7*) Cave (*8*) Road track. The *black rectangles* highlight the detailed study areas

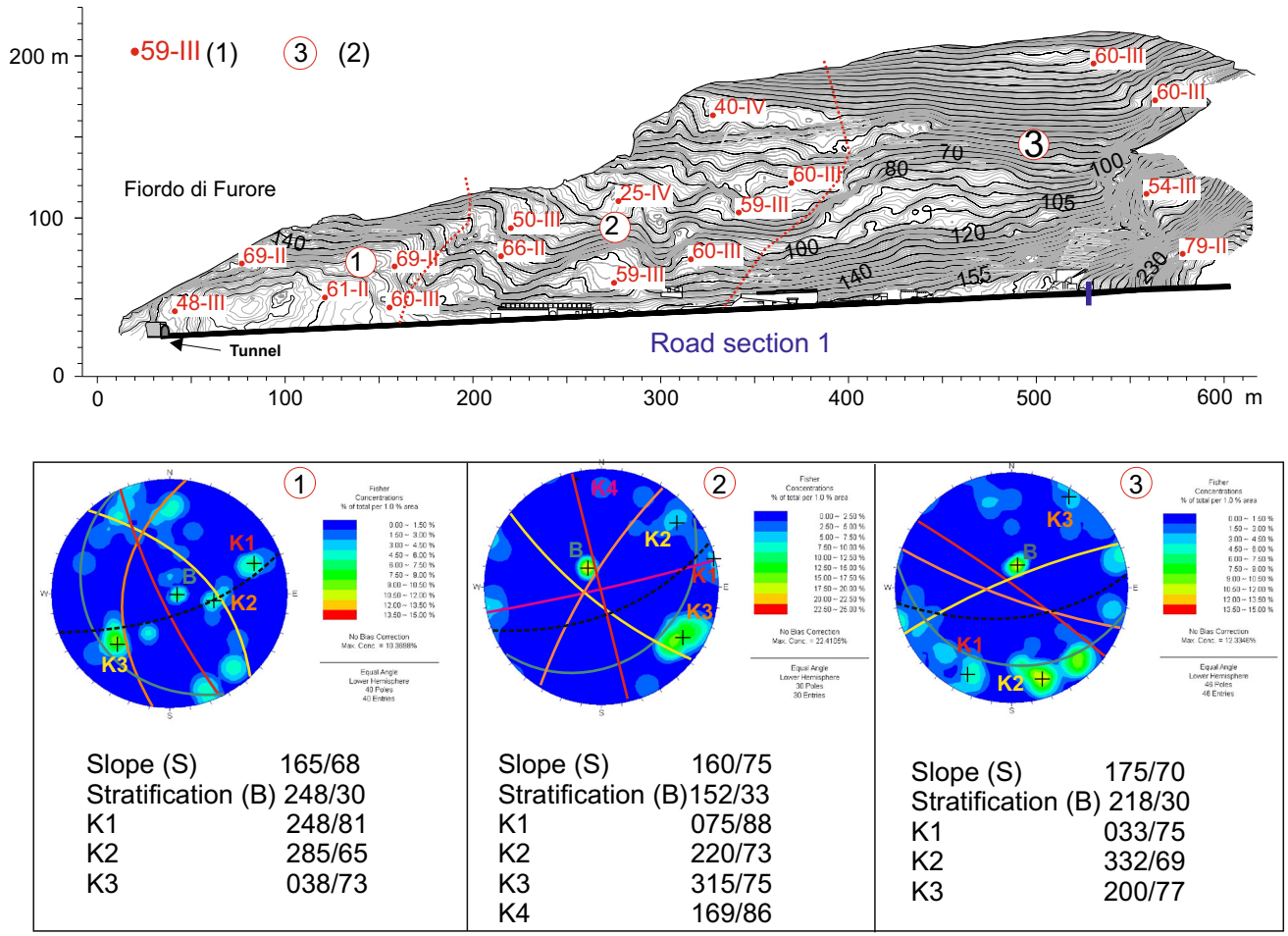

Fig. 9 Photogrammetric map of the slope impending over the road section no 1 (*Fiordo di Furore*) and cyclographic projections of joint sets affecting homogeneous rock mass zones. B—poles of bedding planes; K1... Kn—poles of tectonic joint sets. *Key* (*1*) Location of the geo-mechanical stations with the related SMR value and class according to Romana (1988); (*2*) Homogeneous rock mass sector

each station were processed following Bieniawsky's quali-quantitative criterion, which allowed classification of slopes in geo-mechanical terms using the basic rock mass rating (RMRb) index (Bieniawski 1989). Afterwards, in order to zone slope sectors characterized by different stability and failure mode classes, the slope mass rating (SMR) approach by Romana (1988, 1991) was used. It is useful to point out that the SMR classification introduces evaluation elements of a qualitative nature concerning the type, number, and size of the possible failure modes which were only highlighted on the basis of joint intersections shown by stereonets.

Fiordo di Furore

This slope (Fig. 9), impending over the road section no. 1 and partially on the section no. 2 (Fig. 8), is characterized by heights ranging between 20 and 160 m with a mean value of about 85 m. A predominant steep, sharp-crested profile with scattered thin brushwood indicates an unstable slope affected by gravitative processes. The slope face (dipping on average 60°) coincides with a large fault scarp (NE–SW oriented), caused by tectonic uplifting during the Pliocene and the lower Pleistocene (Bonardi et al. 2009). Discontinuities showing high trace lengths on the surface of exposures (persistence) affect the outcropping rock mass that appears always heavily fractured. On the slope face, limestones crop out that dip to the SE. Joint orientation data was collected at 17 stations allowing subdivision of the whole area into three homogeneous geostructural sectors characterised by different slope face and joint set orientations (Fig. 9). In the sectors 1 and 3, stereonets highlight the presence of four joint sets, which group the bedding planes (B) as well as tectonic discontinuities (K1, K2, and K3) with different mean orientation. In the sector 3, considering the local slope face mean orientation, geometric conditions isolating potentially unstable wedges, due to the joint set intersection K1–K3, as well as plane

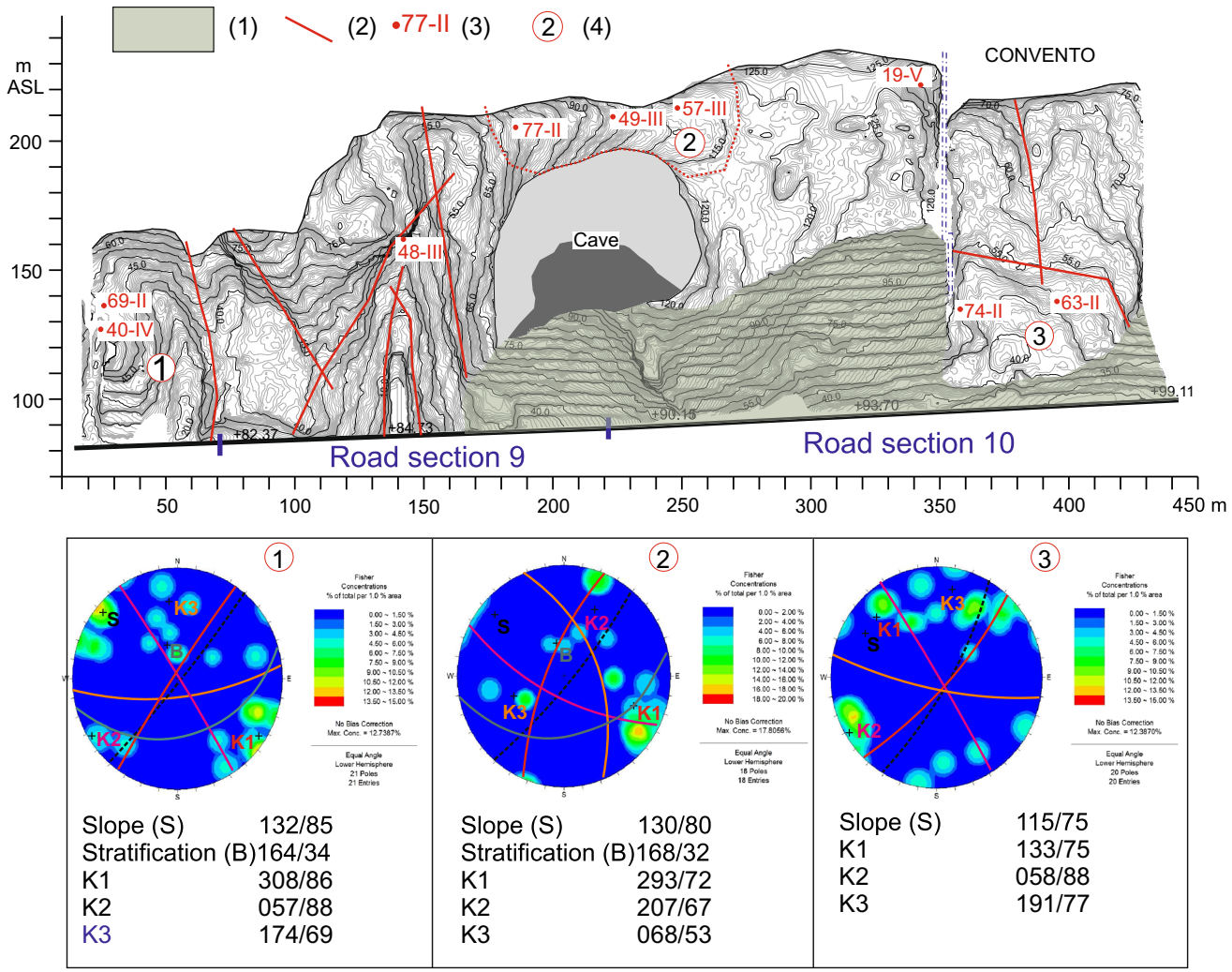

Fig. 10 Photogrammetric map of the slopes impending over the road sections no 9 and 10 (*Convento*) and cyclographic projections of joint sets affecting the homogeneous rock mass zones. B—poles of bedding planes; K1…Kn—poles of tectonic joint sets. *Key 1* Loose rock debris; *2* Main fault; *3* Location of the geo-mechanical stations with the related SMR value and class according to Romana (1988); *4* Homogeneous rock mass sector

failures along bedding planes (B), are kinematically possible. In the sector 2, in addition to the stratification, four tectonic joint sets were detected, which account for a higher jointing degree affecting this area. All the intersections between the four tectonic joint sets, with respect to the local mean slope face orientation (dip direction/dip = 160°/75°), may cause wedge geometries which are kinematically inclined to failure.

The SMR index (Romana 1988), varying between 79 and 25, identifies instability classes ranging from the second ("stable slopes") to the fourth class ("unstable slopes") with a clear prevalence of the third and fourth classes, which are characterized by the presence of "many" (III class) and/or "big" (IV class) possible wedge failures (Fig. 9).

Convento

This slope (Fig. 10), impending over the road sections nos. 9 and 10, is very high reaching a maximum value of about 145 m. Almost everywhere, cliffs are near vertical (dipping on average 80°). In the central sector of this slope, poorly stratified Pleistocene cemented breccias crop out, affected by a wide and very deep cave. Loose landslide debris mixed with weathered pyroclastic sediments crop out at the cavity base (Fig. 7), and were likely caused by relict rockfalls that occurred during the Last Glacial Maximum (LGM) and the mid-Holocene—approximately 20,000 years ago (Di Crescenzo and Santo 2007). Instead, the lateral sectors of the studied slope section are characterised by Mesozoic dolomitic limestones affected by several high trace length faults.

Table 2 Main geo-mechanical properties of rock masses cropping out on slopes impending over the road sections nos. 9 and 10

Geomechanical station (no.)	Joint compressive strength (MPa)	Rock quality designation (%)	Joint roughness coefficient (−)	Average spacing (mm)	Vol. joint count (m^{-1})	Block volume (m^3)	RMRb (−)	SMR (−)	Class (−)
1	117	93	6	438	6.69	0.95	67	40	IV
2	70	89	6	1006	7.88	1.02	72	69	II
3	94	89	3	282	7.78	1.03	68	48	III
4	61	95	6	747	6.10	1.31	72	77	II
5	80	64	6	588	15.35	0.52	64	49	III
6	127	84	6	204	9.51	0.45	66	57	III
7	115	57	8	343	17.69	0.45	64	19	V
8	104	96	8	464	5.69	1.15	68	74	II
9	93	70	8	392	13.64	0.59	68	63	II

Mainly towards SW, the fault intersections isolate high rocky pinnacles impending over the road.

Joint orientation and geo-mechanical data (Fig. 10; Table 2) was collected in nine stations and three homogeneous geostructural sectors, characterised by different slope face and joint set orientations, were identified. In the sector 1, the stereonet highlights the presence of four joint sets which group the bedding planes (B) as well as tectonic discontinuities (K1, K2, and K3) with different mean orientation. Considering the local slope face mean orientation, the joint set intersection K2–K3 identifies potentially unstable geometric wedge conditions, which are upward, truncated by near vertical discontinuities belonging to the joint set K1. The homogeneous geostructural sector 2 marks the slope face corresponding to the vault of the cavity that doesn't show critical joint set intersections. At last, the geostructural sector 3 characterizes the lower portion of the cliff which is located below the *Convento* resort, being upward bounded by a high trace length fault nearly W–E oriented (Fig. 10). All the intersections between tectonic joint sets highlighted by stereonets show probable wedge geometries, with respect to the local slope face mean orientation (dip direction/dip = 115°/75°).

For the whole studied slope, the SMR index varied between 77 and 19, and identifies instability classes ranging from the second ("stable slopes") to the fifth class ("completely unstable slopes") with a clear prevalence of the second and third classes to which it is possible to associate "some block failures" (II class) and/or "many wedge failures" (III class), respectively. Because of the local low values characterizing the Romana joint-slope relationship factors, only in a geo-mechanical station located near the cliff top the rock mass was rated in the fifth class (SMR = 19).

Fig. 11 Small size boulders fallen at the progressive kilometer 26 + 430, on 14th January 2014

Rockfall events

Because of the unfavorable layout of joints, geomorphology, climate, and joint enlargement caused by mechanical stress caused by the roots of the trees, several rockfalls affect cuts and slopes impending over the road stretch that crosses the Conca dei Marini territory (Fig. 11). Starting from the nineteenth century, several historical falls have been recorded testifying the high rockfall susceptibility of this coastal area. Among the data recorded by ANAS (from 2000 to 2008) and the IFFI Catalogue (Progetto IFFI 2010) spanning from 1969 to 2000, a total of 15 rockfall events refer to this area. In such a way, a database reporting the

Table 3 Progressive kilometres where rockfalls occurred

Progressive kilometres	Date
24 + 100	January 2001
24 + 200	March 2008
24 + 600	January 2001
25 + 000	April 2002
25 + 100	October 2004
25 + 300	March 2006
25 + 400	November 1998
25 + 500	October 2001
26 + 300	October 1999
26 + 320	April 2002
26 + 350	November 2000
26 + 400	September 1996
26 + 420	October 2004
26 + 500	December 2002
26 + 650	May 2000

progressive kilometres and dates in which falls happened was prepared, covering a time span from 1996 to 2008 (Table 3). Depending on rainfalls characterized by high-intensity and short-duration, generally occurring during the months of October and November, rockfalls mainly occurred in autumn/winter.

With reference to the time span from 1996 to 2008, a mean rockfall frequency of about 1.15 events year^{-1}, for the entire road stretch, has been calculated. Furthermore, considering the lengths of the ten road stretches, mean rockfall frequency values (λf) ranging between 0 and 1.672 events year^{-1} km^{-1} were evaluated (Table 1). These data can provide a more realistic insight of the hazard level affecting the road (Corominas and Moya 2008).

Since there are no data concerning the volumes of the boulders which reached the road, an attempt was made so as to derive rockfall return periods for assigned volume classes using the landslide magnitude-frequency curves (MFCs). According to Hungr et al. (1999), Dussauge et al. (2003), and Malamud et al. (2004), the MFC for rockfalls can be described by a power law in the following form:

$$\log_{10} N(V) = N_o + b \log_{10} V, \quad (4)$$

where $N(V)$ is the cumulative annual frequency of rockfall events exceeding a given volume class j, No the annual rockfall frequency, and b the power law exponent.

For any given volume class j (i.e. Nj), $N(V)$ can be calculated according to the approach by Hungr et al. (1999). Furthermore, where site-specific magnitude values are missing, for limestone rocks, Agliardi et al. (2009) suggested the use of -0.41 for the exponent b. This value usually varies within a quite narrow range, i.e. $-0.7 < b < -0.4$ (Hungr et al. 1999; Dussauge et al. 2003; Picarelli et al. 2005). With reference to the rockfall inventory, and the mean frequency value of about 1.15 events year^{-1}, return periods varying between about 3.66 and 24 years (for the rockfall magnitude interval between 0.1 and 10 m^3) were computed (Table 4). Caution should be taken when using these data because the used approach is still open to further clarification and it must be considered as a working hypothesis. Furthermore, in the studied site it should be emphasized that several uncertainties spring from the lack of a substantially complete catalogue.

Table 4 Rockfall volume classes, expected frequencies, and return periods according to the adopted magnitude-frequency curves (MFC)

Rockfall magnitude class (m^3)	Annual cumulative frequency (*fi*)	Annual incremental frequency (*fh*)	Return period (years)
0.01	0.447	0.70	1.42
0.1	0.174	0.27	3.66
1	0.068	0.11	9.40
10	0.026	0.04	24.17
100	0.010	0.02	62.13

Rockfall trajectory simulations

In order to apply the RO.MA. method, the number of boulders that may hit the road (Nr) was obtained through trajectory simulations by calculating the percentage of all trajectories that could fall on the road or that are not interfering with it. Based on block volumes of 0.1, 1.0, and 10 m^3 that could break off from slopes and cuts located near the road sections, three rockfall hazard scenarios were analyzed. According to Agliardi et al. (2009), volumes larger than 10 m^3 were not taken into account because they are prone to fragmentation soon after detachment and cannot be considered as single block volumes.

Trajectory simulations were performed using a two-dimensional code (ROCFALL 4.0, by Rocscience Inc. 2002) designed to compute distributions of endpoints, energy, velocity, and bounce-height along slope profiles. Since this program uses a lumped-mass method, boulders are reduced to a single point for the purpose of the analysis, and during the fall possible boulder fragmentations are not considered. Block trajectories depend on energy restitution (normal, RN and tangential, RT) and rolling (friction angle, φ) parameters, whereas they are independent from the shape of the rock. The stochastic nature of rockfall process and the variability of the relevant parameters (slope geometry, energy restitution and rolling friction coefficients, velocities, and slope roughness) are introduced by a Monte Carlo sampling technique that uses a normal distribution. For this

Table 5 Energy restitution coefficients, rolling friction angles, and related standard deviation values adopted for the trajectory simulations performed by means of the ROCFALL code

Material	Normal restitution coefficient (*RN*)	Standard deviation (σ)	Tangential restitution coefficient (*RT*)	Standard deviation (σ)	Friction angle (°)	Standard deviation (σ)
Road asphalt	0.40	0.04	0.90	0.04	30	2
Dolomitic limestones and cemented breccias	0.30	0.04	0.75	0.04	35	2
Loose rock debris mixed with pyroclastic sediments	0.15	0.04	0.35	0.04	40	2

purpose, standard deviation values (σ) for the above-mentioned parameters were used.

In order to use the most suitable *RN*, *RT*, and φ parameters, the back-analysis of previous rockfalls should be performed. In such a case, source areas, impact marks, and trajectory endpoints must be surveyed in great detail. Because of the lack of trajectory data obtainable by the rockfall inventory, reference was made to well-studied trajectory paths of some rockfalls that occurred in the nearby village of Atrani, which is located at 4 km from the studied area (Budetta and Santo 1994). On the basis of approximately 6600 simulated trajectories, kinetic parameters of the outcropping dolomitic limestones and loose rock debris have been established (Table 5).

Using the above-mentioned kinetic parameters along 68 different topographic profiles located in the ten road stretches, simulations were performed for each rockfall hazard scenario. Topographic profiles were drawn using the photogrammetric surveys in the scale 1:500. The sections have been carefully chosen on the basis of the morphology of the area and the starting point for boulders were conventionally located at the highest point of each section (in most cases corresponding with the cliff top). Each simulation consisted of releasing 10,000 blocks from the rockfall source, constantly assuming horizontal and vertical velocities equal to 1.0 and 0.5 m/s, respectively. At this stage, the installed protection devices (Fig. 4) flanking the road that were able to stop and/or alter boulder trajectories, were not taken into account.

Rockfall hazard scenario 1 and related consequences: For a falling block with a volume equal to 0.1 m^3 (return period of about 3.66 years), a hazard scenario based on trajectory endpoints interpolated along topographic profiles has been prepared. In such a way, according to the Rockfall Hazard Assessment Procedure (RHAP) (Mazzoccola and Sciesa 2001), the level of hazard exposure of slopes crossed by the road was expressed in terms of frequency of block transits and endpoints. Only the preliminary longitudinal zonation of the rockfall trajectories provided for this method was performed, dividing the whole area affected by boulders into two different zones exposed to 95 and 100 % frequency of block transits and endpoints, respectively (Fig. 12). These percentages were evaluated on the total amount of blocks released during each simulation, and considering the most unfavorable longitudinal zonation. In such a way, it was possible to check that the percentage of fallen blocks stopping on the road (*Pp*) varies between 0.2 and 0.6 %. Comparing the number of stopped blocks, translational velocities, and total kinetic energies calculated by simulations for the vertical cliffs (sometimes with terraced slopes at the cliff base) and more gentle slopes, it follows that vertical cliffs (where predominant free fall motions happen) are affected by higher block velocities and kinetic energies, than the more gentle slopes (Fig. 13a, a′). Furthermore, the presence of terraced slopes cause higher rebound heights; they, however, rapidly reduce the average translational velocity, forcing a greater number of boulders to stop upstream of the road (Fig. 13b, b′). ROCFALL allowed us also to calculate the cumulative frequency of the arrested blocks and the reach probability as a function of the distance of the road centerline from the source area (Fig. 13c, c′).

According to Jaboyedoff et al. (2005) and Peila and Guardini (2008), the hazard that affects the road (i.e., the number of rocks hitting the road per year and per km) is given by multiplying *Pp* by *Nb* and by the mean failure frequency (λf). In such a way, for the ten studied road sections, it was possible to calculate that *Nr* varies between 1.02 and 5.02 (Table 6).

Considering the potential outcomes (consequences) arising from the detachment of a boulder with a volume of 0.1 m^3, the probability that a passenger has a fatal accident, on a moving vehicle hit by a falling rock, mainly depends on the vehicle position on the road as well the occupied part of the vehicle. It is worth observing that on the entire path of the *Amalfitana* road (from 1853 up to now), owing to a rock that hit the left front door of the car, only one person died on January 1986, travelling from Positano to Praiano (ANAS, unpublished report). According to Bunce et al. (1997), probability values of a fatal accident due to moving vehicle/falling rock and moving vehicle/fallen rock interactions (P2 in the Fig. 3) of 0.2 and 0.1 were assumed, respectively. The probability of a fatal accident due to an impact of a falling rock on a stationary vehicle was

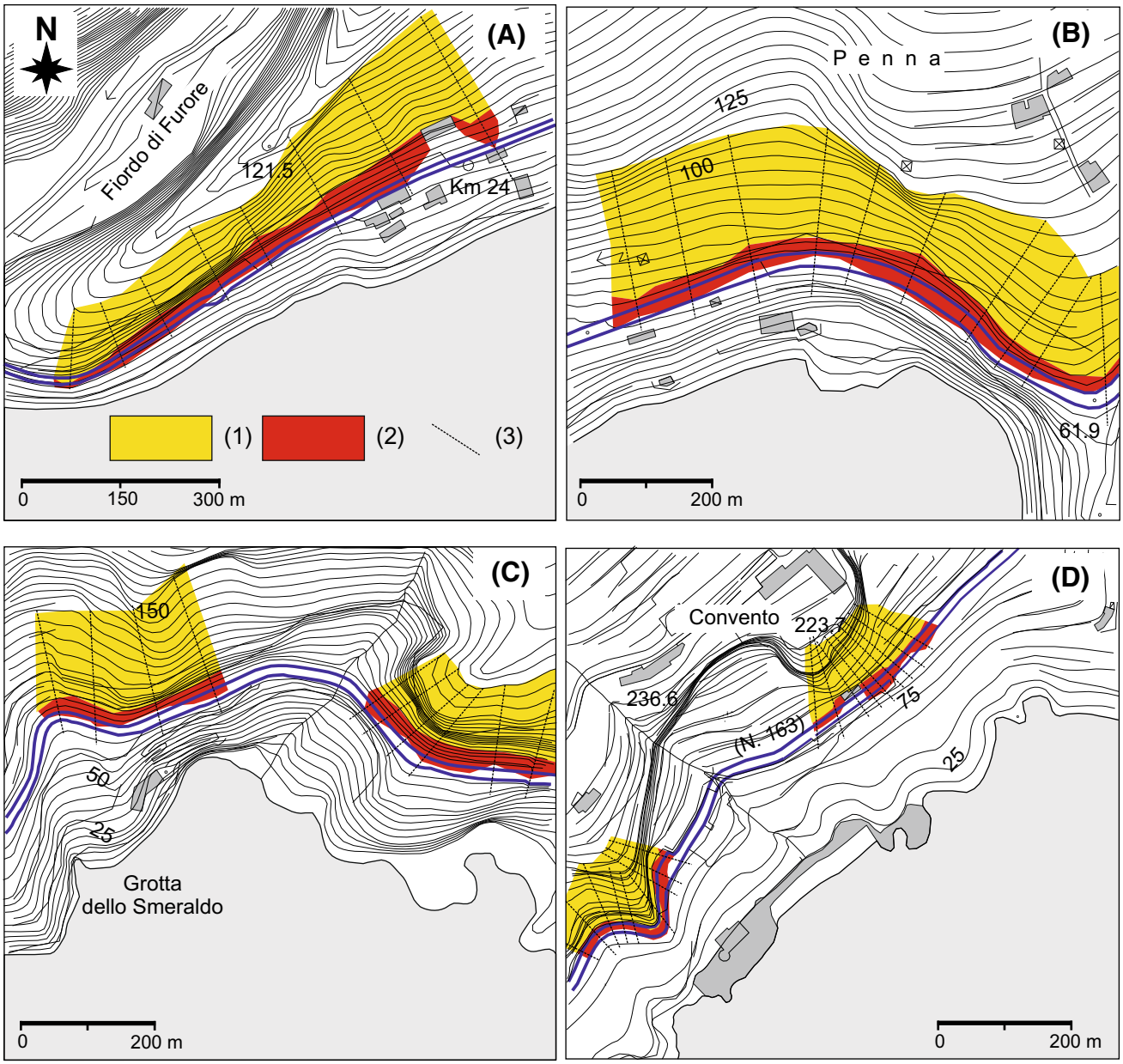

Fig. 12 Hazard scenarios, calibrated on a rockfall volume of 0.1 m^3, for some of the studied areas. *Key 1* zone exposed to transit and stopping of 95 % of blocks, *2* zone exposed to stopping of 100 % of blocks, *3* slope profile. **a** Fiordo di Furore; **b** Penna; **c** San Pancrazio; **d** Pinnacolo and Convento resort. For the location of the studied areas, see the Fig. 6

assumed equal to 0.125 (Bunce et al. 1997). At last, probabilities of serious damage on the road surface (P3 in the Fig. 3) and consequent fatal accident, due to the damaged road surface, are nil. In fact, the available field evidence show that, for rocks with small sizes, the impact marks on the road surface have a slight penetration depth and cannot cause serious damages to vehicles which cross them (Fig. 11).

Rockfall hazard scenario 2 and related consequences: As trajectory paths and types of boulder motion provided by ROCFALL 4.0 are independent from the shape and block mass, it is impossible to outline a different hazard scenario only based on the run-out distances of blocks with different volumes from that already considered in the

Fig. 13 (**a** and **a′**) Trajectory simulations showing endpoints and bounce heights for terraced and gentler slopes at the cliff base, respectively. (**b** and **b′**) Number of stopped blocks (*1*), block velocity (*2*), and total kinetic energy (3) for the shown slopes. (**c** and **c′**) Cumulative frequency of the arrested blocks (*1*) and reach probability (*2*) as a function of the distance of the road centerline from the source area. Graphs refer to simulations performed along a slope profile located in the road Section 10 (block volume equal to 0.1 m^3)

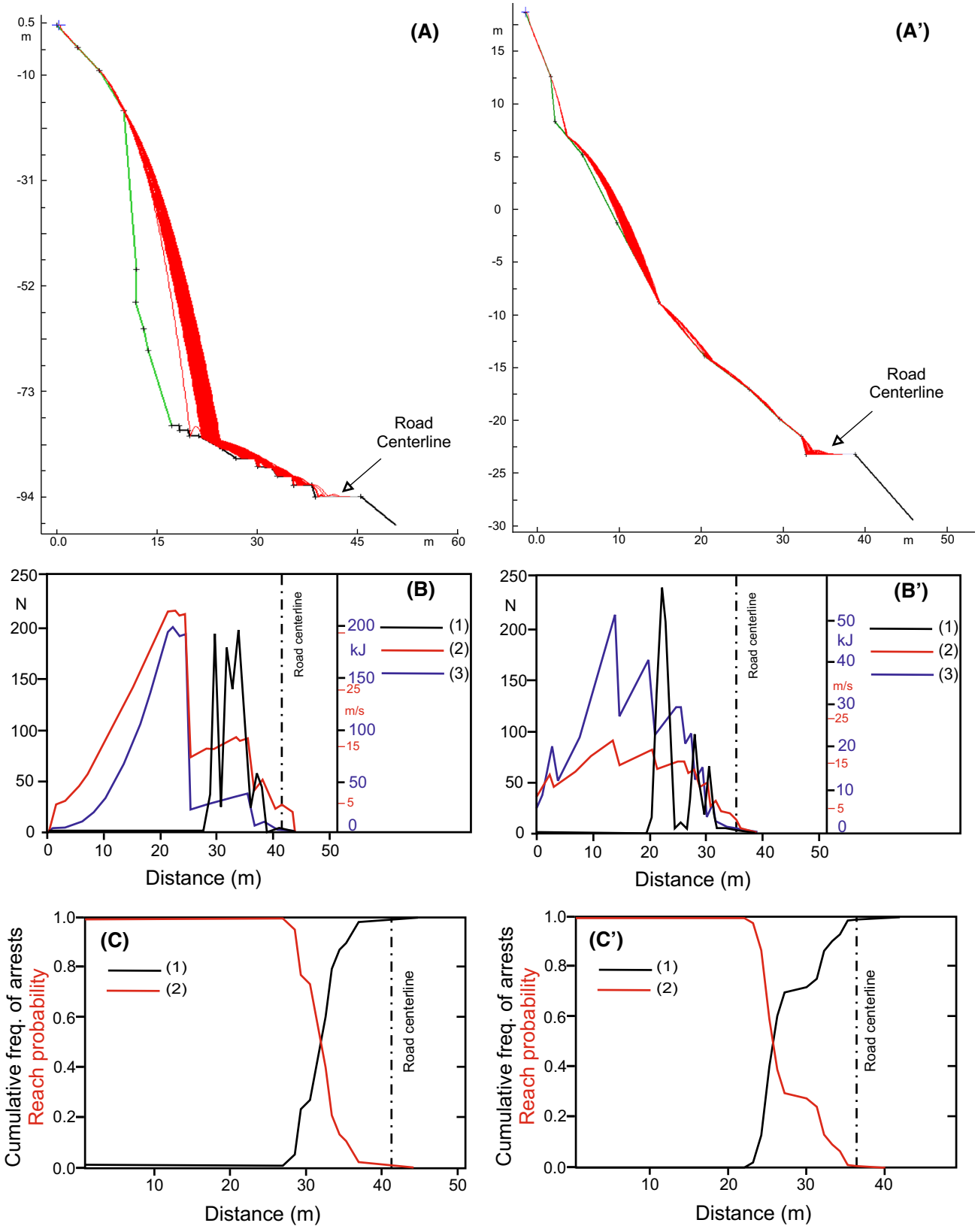
(A)
(A')
Road Centerline
Road Centerline
(B)
(B')
Road centerline
Road centerline
N
kJ
m/s
(1)
(2)
(3)
Distance (m)
Distance (m)
(C)
(C')
Cumulative freq. of arrests
Reach probability
Road centerline
Road centerline
(1)
(2)
Distance (m)
Distance (m)

Table 6 Rockfall events (time span 1996–2008) recorded in the ten road sections, mean failure frequency, and number of rocks hitting the road (per year and per km)

Road section (N)	Rockfall events (N)	λf (events year^{-1} km^{-1})	*Nr* (rocks)
1	1	0.205	1.02
2	1	0.214	1.28
3	1	0.341	2.04
4	0	0	0
5	3	0.824	3.29
6	2	0.496	1.48
7	0	0	0
8	0	0	0
9	5	1.672	5.02
10	2	0.591	1.18

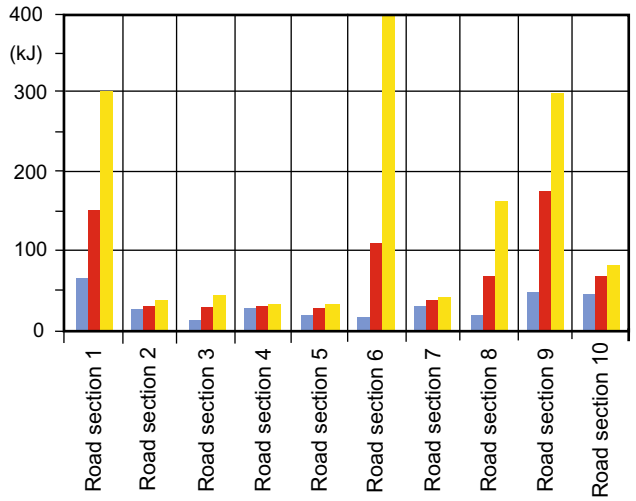

Fig. 14 Minimum, average, and maximum total kinetic energy values affecting rocks (volume of 1.0 m^3) that may hit the road centerline, along the studied road sections

previous case. This means that, apart from block volumes, *Nr* values are always similar. This is a weak point of the used code that we have to consider carefully. Consequently, references were made to total kinetic energies (*Kt*) of blocks of 1.0 m^3 (return period of about 9.40 years) that may hit the road centerline (Fig. 14). Similar average *Kt* values affect the road Sections 2, 3, 4, 5, and 7 (about 30 kJ). On the contrary, along profiles belonging to the road Sects. 6, 8, 9, and 10, average *Kt* values range between 60 and 170 kJ. These higher kinetic energies are linked to higher translational velocities caused by prevalent free fall motions of boulders. For the road Section 1, characterised by a more gentle mean slope, high average *Kt* values can be ascribed to the predominant rolling and rebounding motion of boulders that, breaking off from several low ridges or benches, attain high rotational velocities before impacting on the road. At last, it should be noted that high maximum *Kt* values, detected for the road Sections 6 and 9, can be ascribed to local morphological conditions (such as benches interposed between high cliffs) which causes launching phenomena of boulders formerly affected by free fall motions.

In order to calculate consequences arising from the detachment of a boulder of 1.0 m^3, probability values such as those assumed for the three already analyzed interactions between vehicles and rocks (see the hazard scenario 1) were chosen. On the contrary, due to the larger dimensions of a boulder hitting the road and always causing serious damage to the road surface, a probability value P3 = 1.0 has been heuristically assigned. Consequently, the annual probability of death due to a damaged road surface (P8 in the Fig. 3) is 0.049. This value was obtained from an elaboration of the Italian Institute of Statistics concerning the main causes of road accidents over the years 2003–2004 on the entire Italian road network (Peila and Guardini 2008).

Rockfall hazard scenario 3 and related consequences: With reference to a falling block of 10 m^3 (return period of about 24.17 years) on the road centerline, a more severe hazard scenario based on total kinetic energies can be outlined. Using ROCFALL, average *Kt* values ranging between 350 and 1450 kJ for the ten road sections were calculated. Here too, higher average *Kt* values can be ascribed to prevalent free fall motions affecting boulders that may hit the road Sections 8, 9, and 10. As topographic characteristics and kinetic parameters assumed in trajectory simulations are similar to those already used in the previous scenarios, trajectory paths, and types of motions of rocks are exactly alike. Small differences concerning the run-out distances are only due to the Monte Carlo sampling technique used in ROCFALL.

For the assumed hazard scenario, probability values concerning the three vehicle/rock interactions were: 0.3, 0.2, and 0.2, respectively. Here too, P3 value was assumed equal to 1.0 and the consequent P8 probability value is 0.049.

Risk assessment

Associated with the 12 paths of the event tree, probability values were calculated for the above-mentioned hazard scenarios, using the suggested approach by Peila and Guardini (2008). In order to perform repeated and complex calculations, an Excel spreadsheet was prepared that uses the following input data: the number of rocks hitting the road per year (*Nr*), the length of the hazardous road stretch (*Lr*), the limit speed of the vehicles (*Vv*), the average

vehicle length (*Lv*), the number of vehicles travelling on the road per day (*Nv*), the decision sight distance (*DSD*), as well probability values concerning the serious damage on the road surface (P3 in the Fig. 3) and falling rock stopping on the road (P4). In the case of no severe damage to the road, the value of the probability that a block could either stop or not on the road (P9) was also inserted. In such a way, it was possible to obtain probability values concerning the 12 paths of the event tree. Finally, by the sum of values of identical outcomes, probability values of a fatal accident, non-fatal accident, and no accident were calculated.

Lastly, according to Peila and Guardini (2008), the risk reduction of a fatal accident due to protection devices installed along some of the slopes impending over the road, was calculated. The protection role carried out from the existing rockfall barriers, reinforced wire rope nets, and mesh drapes (Fig. 4) can be expressed by the reduction in the number of falling rocks ($N'r$) that may involve the road, and is given by:

$$N'r = (1 - C)Nr, \tag{5}$$

where C is the catching capacity of the structure, that is, the percentage of rocks that can be stopped by the protection device (Peila and Guardini 2008).

Depending on the type of installed protection, its position on the slope, height, and energy absorption capacity, different C values were adopted (Table 7). According to Mignelli et al. (2014), for rockfall barriers affected by blocks until to 1.0 m^3 an efficacy of 80 % was adopted. As block volumes increase, decreasing retention abilities of the other installed devices were heuristically assumed (Table 7). In fact, it is difficult that the falling blocks assumed in the hazard scenarios 2 and 3 can be restrained only by means of nets, being these protections almost completely inadequate.

Only the road Section 1 is protected for the entire length, whereas the Sections 2, 4, 6, 7, and 9 show percentages of protected lengths varying between 21 and 70 %. For these sections, depending on the real protected lengths, catching capacities of structures were proportionally reduced. All the remaining road sections are unprotected.

Table 7 Catching capacity (in %) of the different protection devices installed along the studied road stretch

Block volume (m^3)	Rockfall barrier[a] (%)	Reinforced wire rope net[b] (%)	Drapery mesh[c] (%)
0.1	80	60	60
1.0	80	50	40
10	50	20	0

[a] Energy absorption capacity: 2000 kJ; nominal height: 4 m

[b] Reinforced double twist hexagonal mesh 80 × 100 mm with wire ropes having diameters between 12 and 20 mm

[c] Nailed steel square-mesh net 200 × 200 mm with wire diameter 8 mm (ANAS, unpublished report)

In such a way, the risk, expressed as the annual probability of a fatal accident, for the three hazard scenarios involving each road section, has been assessed. Results are summarized in Table 8 and Fig. 15 both without and with rockfall protection devices, respectively. For each road section, the total risk is given by the sum of partial risks related to the three hazard scenarios (Table 9). For the protected road sections, the total risk ranges between 0 (road sections nos. 4, 7, and 8) and 1.11×10^{-3} fatalities $year^{-1}$ km^{-1} (road Section 1), whereas for the whole road stretch the computed mean value is 2.24×10^{-3}. It is worth to highlight that for the entirely un-protected road sections (nos. 3, 5, 8, and 10), risk values only depend on variable project block volumes and correlated hazard expressed by Nr values. Obviously, for these un-protected sections is $Nr = N'r$ (Table 8).

According to the abacus, defining values of acceptable and unacceptable rockfall risks (Fig. 2) suggested by Mignelli et al. (2012) for the un-protected road Sect. 1, mainly affected by possible wedge failures with predominant rolling motion of falling boulders, the risk level is acceptable only considering a falling rock of 0.1 m^3. For all remaining scenarios, this risk is always unacceptable. The highest risk values affect the road Sections 6 and 9, with increasing risk levels as more severe hazard scenarios are assumed. Even though during the time span 1996–2008 the Section 9 has been affected by five rockfall events, only about 50 % of cliffs impending over the road have been protected with reinforced wire rope nets, which are not capable of restraining large boulders. Consequently, this section should be protected by means of adequate rockfall barriers. For the road Sections 2 and 6, affected in the past by rockfall events and protected with metallic nets, the risk reduction due to these passive devices is negligible (Fig. 15; Table 9). In our opinion, this derives from the poor efficacy of nets that, in the case of the Section 2, protect less than 25 % of the road length.

Discussion and conclusion

In order to compare risk values calculated by means of RO.MA. method with those concerning all car accidents resulting in life loss in Campania during the time span 1996–2008, available data from the Italian Institute for Statistics (ISTAT 2014) were analyzed (Table 10). With reference to this time interval, a mean value of about 330 fatalities/year or 3.41×10^{-2} fatalities $year^{-1}$ km^{-1} was calculated: the length of the entire Campania road network

Table 8 Fatal accident probability values (no. of fatalities year^{-1} km^{-1}) for different hazard scenarios, without and with rockfall protection devices, for the studied road sections

Road sec. (N)	Road length (km)	*Nr*	Prot. length (Km)	Block volume 0.1 m^3			Block volume 1.0 m^3			Block volume 10 m^3		
				Risk without prot. devices	*Nr'*	Risk with prot. devices	Risk without prot. devices	*Nr'*	Risk with prot. devices	Risk without prot. devices	*Nr'*	Risk with prot. devices
1	0.375	1.02	0.375	9.78×10^{-5}	0.20	3.80×10^{-6}	6.02×10^{-4}	0.20	5.44×10^{-4}	6.34×10^{-4}	0.51	5.64×10^{-4}
2	0.360	1.28	0.075	1.54×10^{-4}	1.17	1.29×10^{-4}	6.37×10^{-4}	1.12	6.14×10^{-4}	6.90×10^{-4}	1.28	6.90×10^{-4}
3	0.225	2.04	0.000	3.85×10^{-4}	2.04	3.85×10^{-4}	7.81×10^{-4}	2.04	7.81×10^{-4}	9.10×10^{-4}	2.04	9.10×10^{-4}
4	0.275	0.00	0.150	0.00	0.00	0.00	0.00	0.00	0.00	0.00	0.00	0.00
5	0.280	3.29	0.000	9.76×10^{-4}	3.29	9.76×10^{-4}	1.15×10^{-3}	3.29	1.15×10^{-3}	1.50×10^{-3}	3.29	1.50×10^{-3}
6	0.310	1.48	0.220	2.01×10^{-4}	1.00	1.92×10^{-4}	6.67×10^{-4}	0.96	5.95×10^{-4}	7.40×10^{-3}	1.30	6.89×10^{-3}
7	0.350	0.00	0.110	0.00	0.00	0.00	0.00	0.00	0.00	0.00	0.00	0.00
8	0.380	0.00	0.000	0.00	0.00	0.00	0.00	0.00	0.00	0.00	0.00	0.00
9	0.230	5.02	0.110	1.45×10^{-3}	4.06	1.19×10^{-3}	1.90×10^{-3}	3.81	1.34×10^{-3}	2.80×10^{-3}	5.00	2.58×10^{-3}
10	0.260	1.18	0.000	1.27×10^{-4}	1.18	1.27×10^{-4}	6.22×10^{-4}	1.18	6.22×10^{-4}	6.63×10^{-4}	1.18	6.63×10^{-4}

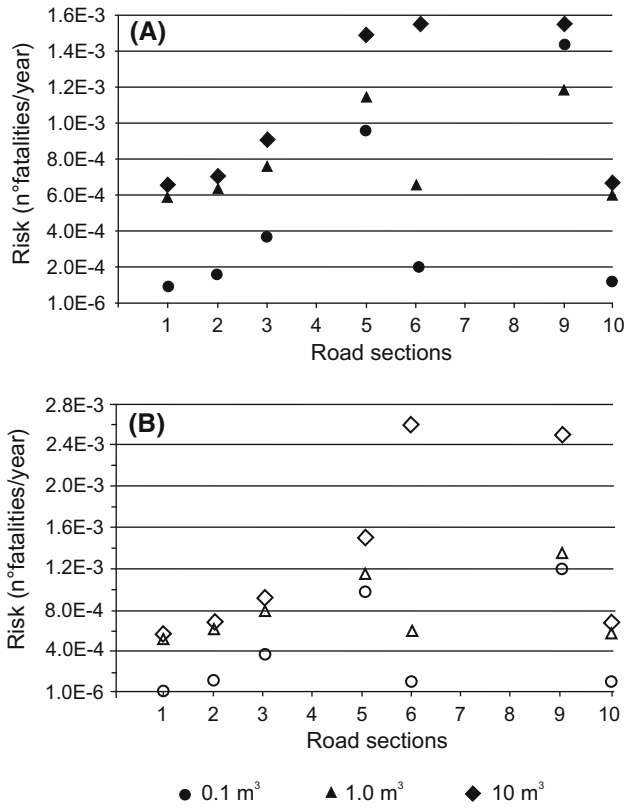

Fig. 15 Risk values for each road section obtained using the RO.MA. method: **a** without rockfall protection devices; **b** with rockfall protection devices

(motorways, national and provincial roads) being about 9652 kilometres. Table 10 shows the variability range between minimum and maximum rockfall risk of a fatal accident for the entire road stretch of the Amalfitana road

Table 9 Total risk (no. of fatalities year^{-1} km^{-1}) for the studied road sections and average values for the entire road stretch, without and with rockfall protection devices

Road section (N)	Total risk without prot. devices	Total risk with prot. devices
1	1.33×10^{-3}	1.11×10^{-3}
2	1.48×10^{-3}	1.43×10^{-3}
3	2.07×10^{-3}	2.07×10^{-3}
4	0.00	0.00
5	3.60×10^{-3}	3.60×10^{-3}
6	8.27×10^{-3}	7.67×10^{-3}
7	0.00	0.00
8	0.00	0.00
9	6.15×10^{-3}	5.11×10^{-3}
10	1.41×10^{-3}	1.41×10^{-3}
Mean value	2.43×10^{-3}	2.24×10^{-3}

without protection devices and taking into account variable efficacy levels of existing devices. The analysis shows that the total risk remains more or less constant, regardless of whether there are any rockfall protection devices. This is also shown by the Fig. 16, where for increasing rockfall magnitude, the risk level doesn't significantly decreases as a result of existing devices. In our opinion, this is due to the wide spread of slopes protected with inadequate restraining metallic nets, characterized by decreasing catching capacities as possible rockfall magnitude increases. It is worth noting (Table 10) that the variable range of rockfall risk is, in both the cases, lower than the risk range of car accidents on the Campania road network and, even though it is unacceptable, it results higher than the real risk of fatal

Table 10 Comparison of risk values (no. of fatalities year^{-1} km^{-1})

	Minimum	Mean	Maximum
Risk of a fatal accident in absence of protection devices	0	2.43×10^{-3}	8.27×10^{-3}
Risk of a fatal accident in presence of protection devices	0	2.24×10^{-3}	7.67×10^{-3}
Risk of fatal car accident in Campania	2.44×10^{-2}	3.41×10^{-2}	4.22×10^{-2}
Real risk of fatal accident caused by rockfalls on the Amalfitana road since its construction			1.65×10^{-4}

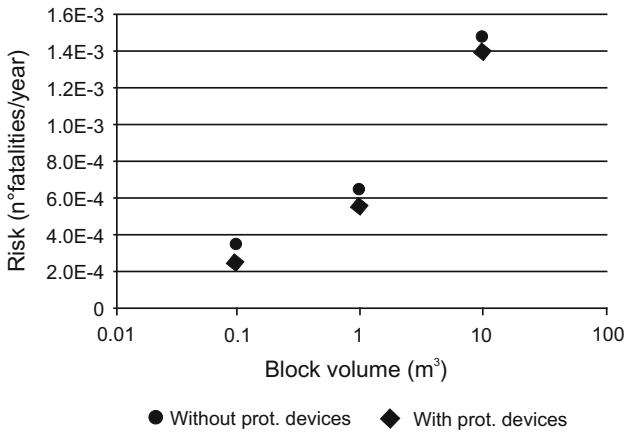

Fig. 16 Average risk values versus block volumes for the entire road stretch, both in absence and presence of rockfall protection devices, respectively

accident caused by rockfalls, on the basis of the fatalities recorded since the construction of the Amalfitana road (1.65×10^{-4} fatalities year^{-1} km^{-1}).

Rockfall risk values are also above the acceptability limit defined for "involuntary" risk such as rockfalls, as proposed by Geotechnical Engineering Office Hong Kong (1998). This means that in the study area, the individual risk is not acceptable, and some actions are requested in order to lower the risk. It must be considered that more effective countermeasures are required such as rockfall barriers and shelters.

With reference to this topic, the analysis suggested that the evaluation of the efficacy of the existing rockfall protection devices must be improved because their effectiveness (catching capacity) was only heuristically assigned (Table 7). Really, in order to evaluate if their energy absorption capacity is suited for catching rocks of different mass and velocity, more detailed studies should be performed, based on both structural data of protection devices and involved kinetic energies. Concerning barriers, Gottardi et al. (2011) developed a numerical procedure to predict the behaviour of barriers installed by ANAS along several hazardous road stretches of the Autonomous Province of Bolzano (Northern Italy) and for which experimental data were not available. Using an FE model of an ANAS semi-flexible barrier prototype, a set of analyses was developed by varying the velocity and mass of impacting blocks in order to identify a threshold level after which the barrier is not able to absorb developed kinetic energy. In such a way, a set of absorption capacities (in kJ) depending on the structural data of the barrier (nominal height, longitudinal rope diameter, impact conditions, etc.) was derived that can be applied to the widely used ANAS barriers (Gentilini et al. 2012; Gottardi et al. 2011). In future, a study should be addressed along these lines. For existing drapery meshes and reinforced wire rope nets, similar studies concerning the chance of obtaining realistic data on the basis of numerical procedures on prototypes are not still available. However, if we consider detaching block volumes of 1 and 10 m^3 it seems unlikely that these can be only restrained from nets.

The rockfall hazard evaluation and the assessment of the total risk performed by means of the RO.MA. method are affected by uncertainties and limitations that we must bear in mind in order to use the results for risk mitigation and planning purposes (Wang et al. 2014). The quality of rockfall hazard scenarios depends on the preciseness of trajectory simulations and the accurate identification of rockfall sources. Energy restitution and rolling friction parameters play a leading role, since affect the evaluation of the number of rocks that may hit the road. The used 2D trajectory simulation code may locally overestimate run-out distances reached from boulders. In fact, due to the lack of field evidence concerning trajectory endpoints and impact marks along slopes, it was not possible to derive the most suitable kinematic coefficients based on the analysis of previous rockfalls. A weak point of the ROCFALL 4.0 code resides in the fact that it doesn't consider the variable shape and mass of rocks. Using codes based on the rigid body approach, more realistic results could be obtained. Also the detachment areas of rockfalls are not always easy to identify and map precisely, so simplifying assumptions sometimes were made, always locating the starting points of boulders on the cliff tops.

With reference to the risk analysis, major difficulties concern the assessment of more exact probability values, which must be assigned to the three interactions between rocks and vehicles. Sometimes the definition of these

values was heuristic, and to some extent arbitrary. With reference to the probability per year of death due to a damaged road surface (P8 in the Fig. 3), the suggested value by Peila and Guardini (2008) doesn't seem to have a good statistical effectiveness because it takes into account only 2 years.

Even though this QRA must be improved, the used approach provides valuable risk values and allows to evaluate the efficiency of passive protection devices and the correctness of their installation. On the basis of the large amount of geostructural and geomechanical data collected in the study area, the used methodology proved that it is possible to perform a good assessment of the expected individual loss of life, for different hazard scenarios, since the results contain the essential elements regarding the evaluation of rockfall hazard and risk exposition.

Acknowledgments The authors are grateful to D. Peila and two anonymous referees for their valuable comments and suggestions that have improved this paper. The authors would also like to thank the Regional Agency Campania Sud that provided many geo-structural and geo-mechanical data.

References

Agliardi F, Crosta GB, Frattini P (2009) Integrating rockfall risk assessment and countermeasure design by 3D modelling techniques. Nat Hazards Earth Syst Sci 9:1059–1073

AGS, Australian Geomechanics Society (2007) Guideline for landslide susceptibility, hazard and risk zoning for land use planning. Aust Geomech 42(1):13–36 **(ISSN 0818-9110)**

Archetti R, Lamberti A (2003) Assessment of risk due to debris flow events. Nat Hazards Rev 4(3):115–125

Bieniawski ZT (1989) Engineering rock mass classifications. Wiley, New York

Bonardi G, Ciarcia S, Di Nocera S, Matano F, Sgrosso I, Torre M (2009) Carta delle principali unità cinematiche dell'appennino meridionale—nota illustrative. It J Geosci 128:47–60 **(in Italian)**

Budetta P (2002) Risk assessment from debris flows in pyroclastic deposits along a motorway, Italy. Bull Eng Geol Env 61:293–301

Budetta P, Nappi M (2013) Comparison between qualitative rockfall risk rating systems for a road affected by high traffic intensity. Nat Hazards Earth Syst Sci 13:1643–1653

Budetta P, Santo A (1994) Morphostructural evolution and related kinematics of rockfalls in Campania (southern Italy): a case study. Eng Geol 36:197–210

Bunce CM, Cruden DM, Morgenstern NR (1997) Assessment of the hazard from rockfall on a highway. Can Geotech J 34:344–356

Cantarella GE, De Luca S (2006) Studio della mobilità in Costiera Amalfitana per un sistema integrato di trasporto collettivo, Research report, Department of Civil Engineering, University of Salerno, Italy, p 105 (**in Italian**)

Corominas J, Moya J (2008) A review of assessing landslide frequency for hazard zoning purposes. Eng Geol 102:193–213

Corominas J, van Westen C, Frattini P, Cascini L, Malet JP, Fotopoulou S, Catani F, Van Den Eeckhaut M, Mavrouli O, Agliardi F, Pitilakis K, Winter MG, Pastor M, Ferlisi S, Tofani V, Hervàs J, Smith JT (2014) Recommendations for the quantitative analysis of landslide risk. Bull Eng Geol Environ 73:209–263

Dai FC, Lee CF, Ngai YY (2002) Landslide risk assessment and management: an overview. Eng Geol 64:65–87

Di Crescenzo G, Santo A (2007) High-resolution mapping of rock fall instability through the integration of photogrammetric, geomorphological and engineering–geological surveys. Quatern Int 171–172:118–130. doi:10.1016/j.quaint.2007.03.025

Dussauge C, Grasso JR, Helmstetter A (2003) Statistical analysis of rockfall volume distributions: implications for rockfall dynamics. J of Geoph Res 108(B6):2286. doi:10.1029/2001JB000650

Fell R, Ho KKS, Lacasse S, Leroi E (2005) A framework for landslide risk assessment and management. In: Hungr O, Fell R, Couture R, Eberhardt E (eds) Proc landslides risk management. Taylor and Francis Group, London, pp 3–26 **(ISBN: 04 1538 043X)**

Ferlisi S, Cascini L, Corominas J, Matano F (2012) Rockfall risk assessment to persons travelling in vehicles along a road: the case study of the Amalfi coastal road (southern Italy). Nat Hazards 62:691–721

Gentilini C, Govoni L, de Miranda S, Gottardi G, Ubertini F (2012) Three-dimensional numerical modelling of falling rock protection barriers. Comput Geotech 44:58–72

Geotechnical Engineering Office (1998) Landslides and boulder falls from natural terrain: interim risk guidelines. GEO report no. 75. Geotechnical Engineering Office, The Government of the Hong Kong Special Administrative Region: p 183

Gottardi G, Govoni L, Mentani A, Ranalli M, Strada C (2011) The effectiveness of protection systems toward rockfall risk mitigation. In: Vogt NB, Schuppener B. (eds) Proc. 3rd int symp on geotech safety and risk. By edited Straub and Bräu, 157–164, ISBN 978-3-939230-01-4

Guzzetti F, Reichenbach P, Ghigi S (2004) Rockfall hazard and risk assessment along a transportation corridor in the Nera Valley, central Italy. Environ Manag 34(2):191–208

Hungr O, Evans SG, Hazzard J (1999) Magnitude and frequency of rock falls and rock slides along the main transportation corridors of south-western British Columbia. Can Geotech J 36:224–238

ISRM (2007) The complete ISRM suggested methods for rock characterization, testing and monitoring: 1974–2006. In: Ulusay R, Hudson JA (eds) Suggested methods prepared by the commission on testing methods. International society for rock mechanics, compilation arranged by the ISRM Turkish National Group, Ankara, Turkey

ISTAT, Italian Institute for Statistics (2014) Anno 2013 incidenti stradali in Campania. Statistiche focus. http://www.istat.it. Accessed 18 Jan 2015 (in Italian)

Jaboyedoff M, Dudt JP, Labiouse V (2005) An attempt to refine rockfall hazard zoning based on the kinetic energy, frequency and fragmentation degree. Nat Hazards Earth Syst Sci 5:621–632

Jaiswal P, van Westen CJ (2013) Use of quantitative landslide hazard and risk information for local disaster risk reduction along a transportation corridor: a case study from Nilgiri district, India. Nat Hazards 65:887–913

Malamud BD, Turcotte DL, Guzzetti F, Reichenbach P (2004) Landslide inventories and their statistical properties. Earth Surf Proc Land 29:687–711

Mazzoccola D, Sciesa E (2001) La metodologia RHAP (Rockfall hazard assessment procedure). Prevenzione dei fenomeni di instabilità delle pareti rocciose, Programme Interreg II C: 84–95 (**in Italian**)

Michoud C, Derron MH, Horton P, Jaboyedoff M, Baillifard FJ, Loye A, Nicolet P, Pedrazzini A, Queyrel A (2012) Rockfall hazard and risk assessments along roads at a regional scale: example in Swiss Alps. Nat Hazards Earth Syst Sci 12:615–629

Mignelli C, Lo Russo S, Peila D (2012) Rockfall risk management assessment: the RO.MA. approach. Nat Hazards 62:1109–1123

Mignelli C, Peila D, Lo Russo S, Ratto SM, Broccolato M (2014) Analysis of rockfall risk on mountainside roads: evaluation of the effect of protection devices. Nat Hazards 73:23–35

Ministerial Decree 5/11/2001, no. 6972: Norme funzionali e geometriche per la costruzione delle strade, Ministero delle Infrastrutture e dei Trasporti, Gazzetta Ufficiale del 04/01/2002 n. 3, p 90 (in Italian)

Palmstörm A (1996) The rock mass index (RMI) applied in rock mechanics and rock engineering. J Rock Mech Tunn Technol 11:1–4

Peila D, Guardini C (2008) Use of the event tree to assess the risk reduction obtained from rockfall protection devices. Nat Hazards Earth Syst Sci 8:1441–1450

Picarelli L, Oboni F, Evans SG, Mostyn G, Fell R (2005) Hazard characterization and quantification. In: Hung O, Fell R, Couture R, Eberhardt E (eds) Proc. landslide risk management. Taylor and Francis Group, London, pp 27–61 **(ISBN: 04 1538 043X)**

Progetto IFFI (2010) Inventario dei fenomeni franosi in Italia. http://www.isprambiente.gov.it/it/progetti/suolo-e-territorio-1/iffi-inventario-dei-fenomeni-franosi-in-italia. Accessed 15 Jan 2015 (in Italian)

Roberds W (2005) Estimating temporal and spatial variability and vulnerability. In: Hungr O, Fell R, Couture R, Eberhardt E (eds) Proc. landslide risk management. Taylor and Francis Group, London, pp 3–26 **(ISBN: 04 1538 043X)**

Rocscience Inc.: ROCFALL v. 4.0 (2002) Statistical analysis of rockfalls. Software tools for rock and soil, Toronto, Ontario, Canada

Romana M (1988) Practice of SMR classification for slope appraisal. Proc 5th int symp on landslides, Balkema, Rotterdam, 1227–1229

Romana M (1991) SMR Classification. Proc 7th int congr on rock mech Balkema, Rotterdam, 955–960

Wang X, Frattini P, Crosta GB, Zhang L, Agliardi F, Lari S, Yang Z (2014) Uncertainty assessment in quantitative rockfall risk assessment. Landslides 11:711–722